A THEMIS multicase study of dipolarization fronts in the magnetotail plasma sheet

A. Runov,[1] V. Angelopoulos,[1] X.-Z. Zhou,[1] X.-J. Zhang,[1] S. Li,[1] F. Plaschke,[2] and J. Bonnell[3]

[1] We discuss results of a superposed epoch analysis of dipolarization fronts, rapid ($\delta t < 30$ s), high-amplitude ($\delta B_z > 10$ nT) increases in the northward magnetic field component, observed during six Time History of Events and Macroscale Interactions during Substorms (THEMIS) conjunction events. All six fronts propagated earthward; time delays at multiple probes were used to determine their propagation velocity. We define typical magnetic and electric field and plasma parameter variations during dipolarization front crossings and estimate their characteristic gradient scales. The study reveals (1) a rapid 50% decrease in plasma density and ion pressure, (2) a factor of 2–3 increase in high-energy (30–200 keV) electron flux and electron temperature, and (3) transient enhancements of ~5 mV/m in duskward and earthward electric field components. Gradient scales of magnetic field, plasma density, and particle flux were found to be comparable to the ion thermal gyroradius. Current densities associated with the B_z increase are, on average, 20 nA/m^2, 5–7 times larger than the current density in the cross-tail current sheet. Because $\mathbf{j} \cdot \mathbf{E} > 0$, the dipolarization fronts are kinetic-scale dissipative regions with Joule heating rates of 10% of the total bursty bulk flow energy.

1. Introduction

[2] Multispacecraft observations of earthward propagating, front-like increases in the northward magnetic field component (B_z) in the near-Earth plasma sheet have been reported for 30 years [*Russell and McPherron*, 1973; *Moore et al.*, 1981; *Angelopoulos et al.*, 1992; *Ohtani et al.*, 1998; *Ohtani*, 1998; *Nakamura et al.*, 2002b]. Superposed epoch analyses of Geotail observations have shown that transient dipolarizations observed near the leading edge of earthward fast flows include a sharp increase in the northward magnetic field component (B_z), preceded by a smaller amplitude, negative B_z variation [*Ohtani et al.*, 2004]. These asymmetric bipolar B_z variations with a typical time scale of 1 min were observed in a large portion of the magnetotail plasma sheet between $X = -30$ and -5 R_E. A sharp B_z increase, often referred as to a dipolarization front [e.g., *Nakamura et al.*, 2002b; *Sitnov et al.*, 2009], is also a common feature of flow bursts within bursty bulk flow (BBF) events [*Angelopoulos et al.*, 1994].

[1]Institute of Geophysics and Planetary Physics, University of California, Los Angeles, California, USA.
[2]Institut für Geophysik und Extraterrestrische Physik, Technische Universität Braunschweig, Braunschweig, Germany.
[3]Space Sciences Laboratory, University of California, Berkeley, California, USA.

[3] Recent observations by Time History of Events and Macroscale Interactions during Substorms (THEMIS) [*Angelopoulos*, 2008] probes distributed along the magnetotail have revealed that dipolarization fronts with $\delta B_z > 20$ nT propagate as coherent structures with thickness comparable to an ion thermal gyroradius over a macroscopic distance up to 10 R_E (hundreds of ion inertial lengths) in a few minutes (tens to one hundred ion gyroperiods) [*Runov et al.*, 2009]. Thus, dipolarization fronts are microscale structures with a macroscale lifetime. *Runov et al.* [2009] also showed high-energy ion and electron flux increases at the front. Assuming constant front propagation velocity and converting time to space, *Runov et al.* [2011] estimated current density associated with rapid B_z increase to be as high as 50–100 nA/m^2. *Sergeev et al.* [2009] reported observation of a dipolarization front propagating inward between 11 and 9 R_E with a 50 mV/m electric field confined to a thin layer at the front.

[4] Previous event studies have shown ion pressure and bulk velocity increases about 1 min prior to dipolarization front crossing [*Sergeev et al.*, 2009; *Runov et al.*, 2011]. These velocity and pressure enhancements were suggested to be due to (1) remote sensing of the approaching dipolarization front by ambient plasma sheet ions [*Zhou et al.*, 2010, 2011] and/or (2) compression of ambient plasma by the approaching dipolarized flux tube [*Li et al.*, 2011].

[5] Earthward moving, bipolar B_z variations with a time scale of a few to several tens of seconds observed in the

Table 1. Probe Positions, Minimum Variance Analysis, and Timing Results[a]

Spacecraft	t_0 (UT)	Spacecraft Position (GSM, R_E)	MVAB λ	MVAB N	V_t (km/s)
		27 February 2009 Event			
THB	0751:25.60	−20.1, −0.6, −1.5	76.5, 6.02, 0.13	0.88, −0.25, −0.40	
THC	0752:34.40	−16.7, −1.6, −2.2	107.0, 8.93, 0.17	0.79, −0.43, −0.43	300
THD	0754:06.60	−11.1, −2.7, −2.1	102.3, 4.64, 0.72	0.54, −0.09, 0.84	350
THE	0754:10.30	−11.1, −1.8, −2.4	153.2, 1.90, 0.04	0.22, 0.83, 0.51	350
		5 March 2009 Event			
THC	0313:04.10	−17.9, 1.4, −1.6	23.9, 7.79, 0.14	0.45, 0.24, −0.86	
THD	0314:26.77	−10.3, 1.5, −1.7	132.6, 1.27, 0.06	0.92, −0.39, 0.09	500
THA	0314:33.75	−9.1, 2.4, −2.3	174.8, 17.64, 0.23	0.65, 0.23, −0.72	
THE	0314:38.50	−9.2, 2.4, −1.5	166.4, 25.4, 0.29	0.93, 0.33, −0.13	500
		9 March 2009 Event			
THC	0906:49.00	−14.3, −0.8, −1.2	30.4, 0.77, 0.06	0.83, −0.53, −0.17	
THE	0907:45.10	−11.4, −1.2, −1.6	17.3, 1.52, 0.03	0.99, −0.07, −0.15	300
THD	0907:58.70	−11.1, −2.1, −1.3	20.9, 0.45, 0.06	0.53, −0.84, −0.08	300

[a]Here t_0 UT indicates onset of the positive B_z variations. MVA was performed over a variable window around the specified UT. Results with the best ratio of λ_2 and λ_3 are shown.

inner plasma sheet have been typically interpreted either as BBF-type flux ropes [*Slavin et al.*, 2003] or as nightside flux transfer events (NFTE) [*Sergeev et al.*, 1992]. The flux rope interpretation, based on the multiple X line concept, assumes two active X lines separated by an O-type neutral line [see *Slavin et al.*, 2003, Figure 12b]. Spacecraft crossing the earthward moving flux rope will detect first negative then positive B_z, with maximum negative B_z variation at the magnetic equator ($B_x = 0$). In a case of oblique crossing, the B_z variation may be fairly asymmetric. The NFTE concept is based on an MHD model of impulsive reconnection at a unique X line [e.g., *Semenov et al.*, 2005]. In this case, the probability of observing a negative B_z dip increases with increasing distance from the magnetic equator. In the neutral sheet ($B_x \approx 0$), B_z may touch zero level, but does not change its sign. Although magnetic field signatures of flux ropes and NFTEs may look identical, plasma properties at these two objects differ; the differences are most pronounced in energetic electron flux distributions. Within a flux ropes, which are formed by multiple reconnection, hot electrons are confined within a topologically closed magnetic structure [e.g., *Zong et al.*, 2004]. A probe crossing the flux rope detects a hot electron flux profile that is approximately

symmetric with respect to the magnetic bipolar structure center enhancement. In contrast, an NFTE is a boundary separating accelerated (presumably freshly reconnected) plasma from the ambient plasma sheet population. In this case, a probe crossing this boundary close to the magnetic equator records a hot electron flux profile with a more or less sharp increase immediately after the positive jump in B_z [*Sormakov and Sergeev*, 2008]. Examination of magnetic field configuration and energetic electron fluxes around dipolarization fronts will help distinguish between flux ropes and NFTE-type structures and address the question of front origin.

[6] Systematic multicase studies are needed to confirm results from previous event studies. They may also reveal common patterns in field and plasma parameter variations around dipolarization fronts. To distinguish spatial structures from temporal variations, it is important to select events in which the front is detected by several probes distributed along the magnetotail. A front propagation velocity obtained from multipoint timing along with front orientation established by variance analysis enable estimation of field and plasma gradients at the front.

[7] In this paper we discuss the results of a multicase study of dipolarization fronts detected by at least three

Table 2. Same as in Table 1

| Spacecraft	t_0 (UT)	Spacecraft Position (GSM, R_E)	MVAB λ	MVAB <u>N</u>	V_t (km/s)
		15 March 2009 Event			
THC	0849:05:08	−13.7, 0.1, −0.9	44.7, 1.61, 0.06	0.98, 0.21, 0.07	
THB	0849:11.35	−12.6, 0.1, −0.2	32.9, 0.59, 0.07	0.46, −0.85, −0.25	
THA	0849:19.30	−11.5, −0.2, −2.3	47.9, 1.41, 0.02	0.71, −0.34, −0.62	
THE	0849:28.00	−11.5, −0.2, −1.3	35.3, 1.0, 0.14	0.96, 0.18, −0.21	600
THD	0849:38.05	−11.3, −1.1, −1.0	28.5, 2.07, 0.03	0.94, −0.35, −0.07	450
		19 March 2009 Event			
THC	0825:11.50	−13.4, 0.7, −0.6	81.4, 13.8, 0.18	0.91, 0.39, −0.14	
THB	0825:19.20	−12.3, 0.7, 0.0	80.1, 2.03, 0.64	0.68, −0.14, −0.72	
THE	0825:30.10	−11.5, 0.6, −1.1	80.6, 5.38, 0.05	0.96, 0.05, −0.32	550
THD	0825:33.10	−11.4, −0.3, −0.9	51.8, 2.48, 0.42	0.72, −0.26, 0.64	550
		31 March 2009 Event			
THD	0825:47.50	−11.2, 1.2, −0.1	180.9, 2.47, 0.21	0.95, 0.27, 0.18	
THC	0825:50.00	−11.1, 1.5, 0.0	178.2, 4.05, 0.18	0.89, 0.42, 0.16	300
THE	0825:58.25	−11.3, 2.2, −0.4	44.7, 4.78, 0.14	0.48, 0.87, 0.13	
THB	0826:09.17	−9.6, 1.2, 0.4	28.02, 0.57, 0.03	0.69, 0.71, 0.12	
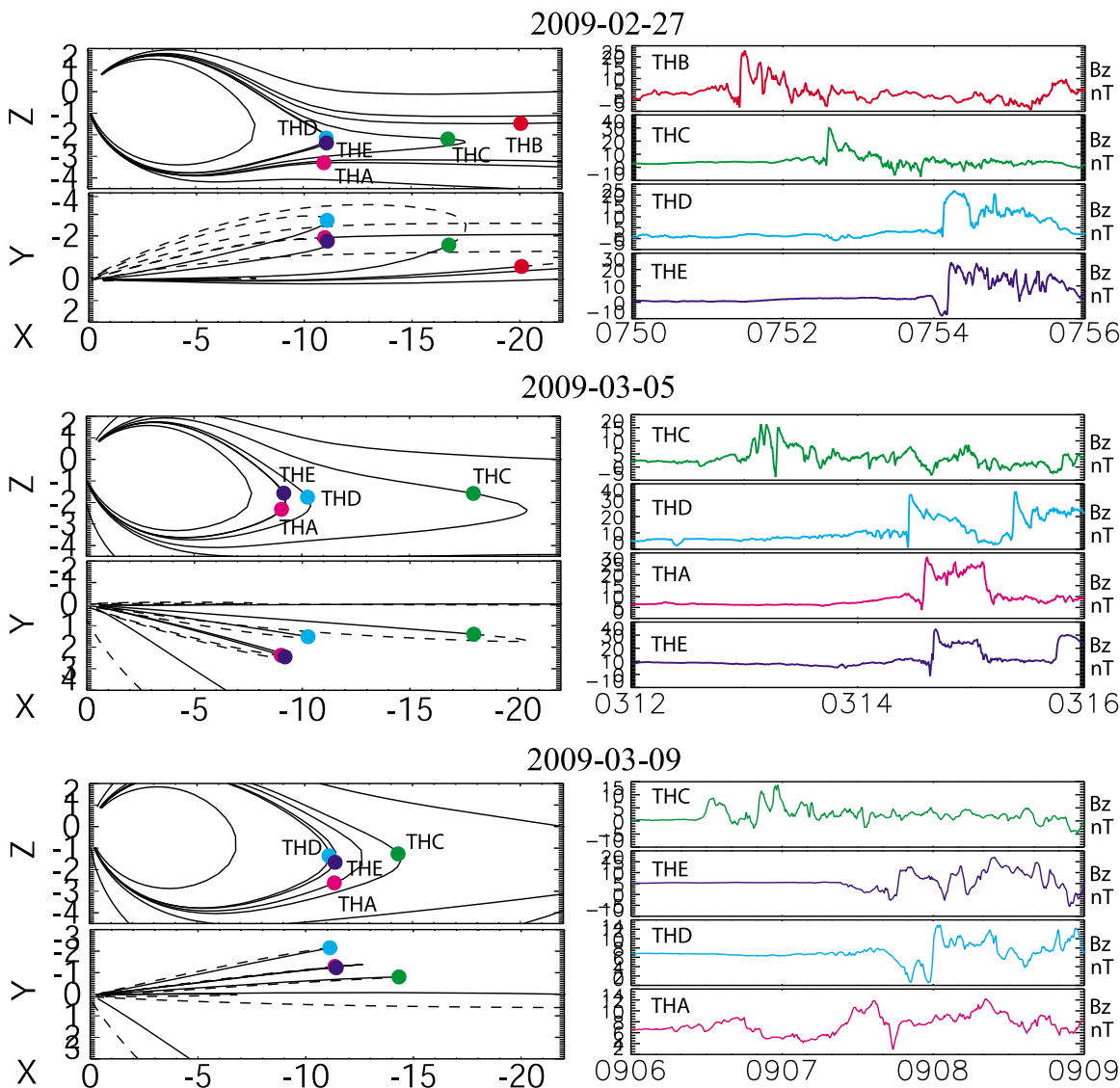
Figure 1. (left) THEMIS probe positions and T96 model [*Tsyganenko*, 1995] magnetic field lines in (*XZ*) and (*XY*) GSM planes for 27 February, 5 March, and 9 March 2009 events. (right) *Z* GSM component of the magnetic field versus UT.

probes. We analyze variations in magnetic and electric fields, plasma moments, and particle and energy fluxes detected during front crossings and identify (1) common, robust, field and plasma variation patterns and (2) typical field and plasma gradient scales at dipolarization fronts. This information is essential for understanding the physics of dipolarization front formation and evolution and the role of fronts in energy transport in the magnetotail. The aim of this paper is to reveal common patterns; variations in signatures observed at different positions will be discussed in separate publications.

2. Instrumentation

[8] Each THEMIS probe carries identical instrumentation [*Angelopoulos*, 2008]. Data from the following instruments are used in this study: (1) the Fluxgate Magnetometer (FGM) [*Auster et al.*, 2008], which provides DC magnetic field measurements with a temporal resolution of 128 vectors per second during the burst mode; (2) the Electric Field Instrument (EFI) [*Bonnell et al.*, 2008], which measures electric field with the sample rate 0.125 Hz; (3) the Electrostatic Analyzer (ESA) [*McFadden et al.*, 2008], which provides ion and electron distribution functions in the energy range from 5 eV up to 25 keV with a time resolution of 1 3-D distribution function per spin in the burst mode; and (4) the Solid State Telescope (SST) [*Angelopoulos*, 2008], which detects high-energy (25 keV to 1 MeV) ion and electron fluxes with a time resolution of 1 3-D distribution function per spin in the burst mode.

3. Data Analysis

[9] To select events for this study, the THEMIS major and minor (i.e., when all five or just four probes, respectively, were situated in the magnetotail and separated by less than 2
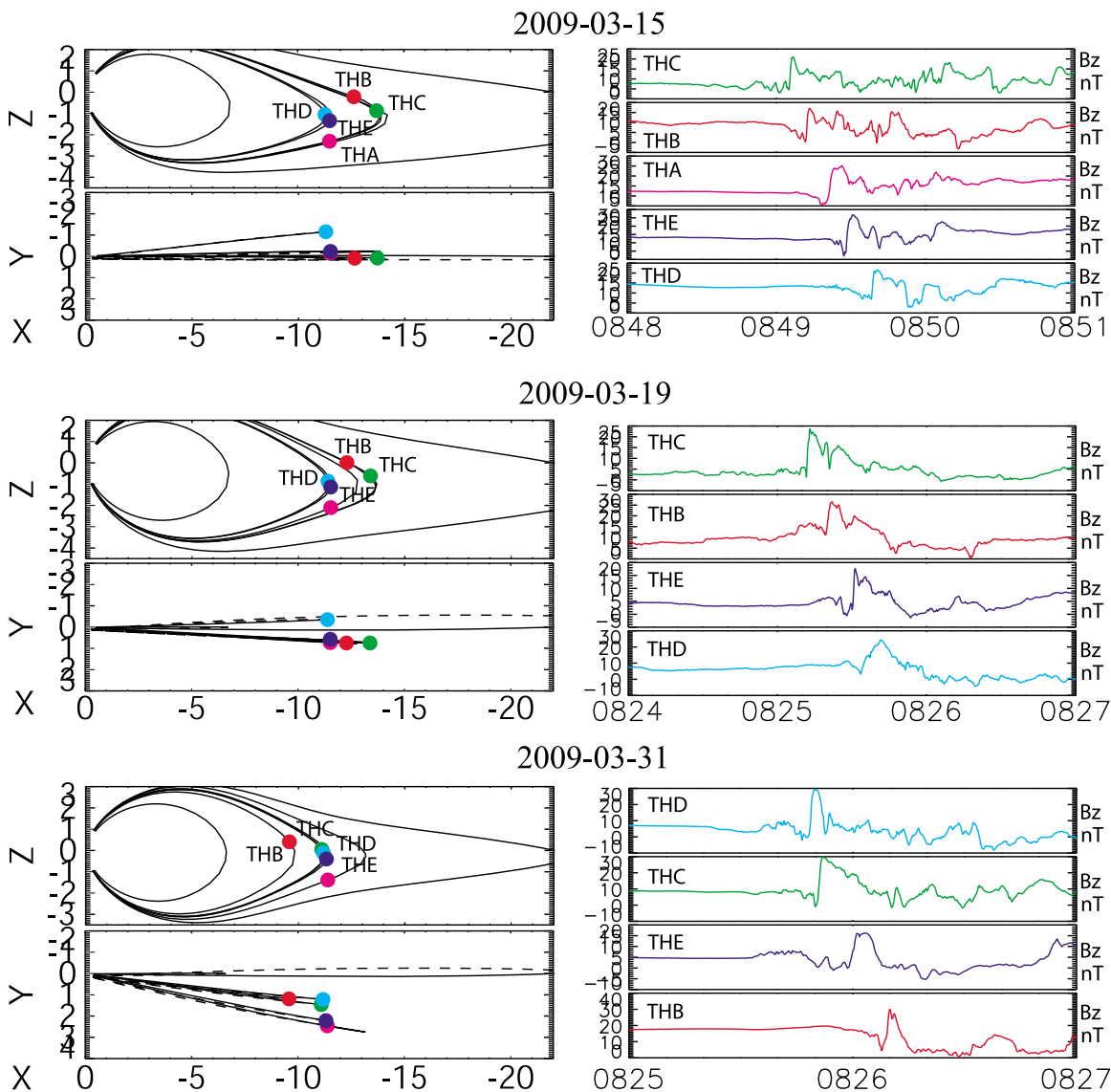
Figure 2. Same as in Figure 1 but for 15, 19, and 31 March 2009 events.

R_E in the cross-tail direction) conjunction intervals in 2009 tail season (mid-December–April) were used. The selection criteria were the following: (1) plasma-beta $\beta = \mu_0 P_p B^{-2} > 1$ at least 10 min prior to the variation in B_z, indicating front arrival; (2) Bz variation amplitude $\delta B_z > 10$ nT within the time interval $\delta t < 30$ s indicating front crossing; and (3) absence of large-amplitude (>5 nT) B_z variations for 2 min preceding front crossing. The first criterion ensures that the probe is located in the central plasma sheet; the second and the third are used to select dipolarization fronts. Application of these criteria to the observations resulted in a large number of events (>100). From them, events detected by at least 3 probes were selected. Finally, to ensure accurate multipoint timing, cases with distinct front onsets were selected for analysis. The selection resulted in the six cases listed in Tables 1 and 2.

[10] Figures 1 and 2 show THEMIS probe configurations (left panel) in the XZ and XY GSM planes and B_z time series at the probes situated in the plasma sheet. The events are indicated by their dates. The letter identifications (THA,

THB, THC, THD, and THE) and colors (magenta, red, green, cyan, and blue, respectively) are used for probes and corresponding field time series. The THEMIS configuration varies event by event from tail-aligned (27 February, 5 March, and 9 March 2009) to cluster-like constellations (15, 19, and 31 March 2009). The probe coordinates and times of the positive B_z variations onsets, used as the "epoch zero" (t_0) in the following superposed epoch analysis, are listed in Tables 1 and 2.

[11] The B_z time series (except for one at THA on 9 March 2009) show similar signatures: a large amplitude, positive variation often preceded by a smaller amplitude, negative variation. Time delays of the B_z signatures indicate their propagation from the most tailward probe to near-Earth ones, i.e., inward. The B_z time series at THA on 9 March 2009 shows that the front is vertically localized: THA, situated 1 R_E southward of THE and THD (see probe coordinates listed in Tables 1 and 2) did not detect the front. Front velocities (V_t) were estimated using time delays between front onsets at THC, THD, and THE (except for the 27
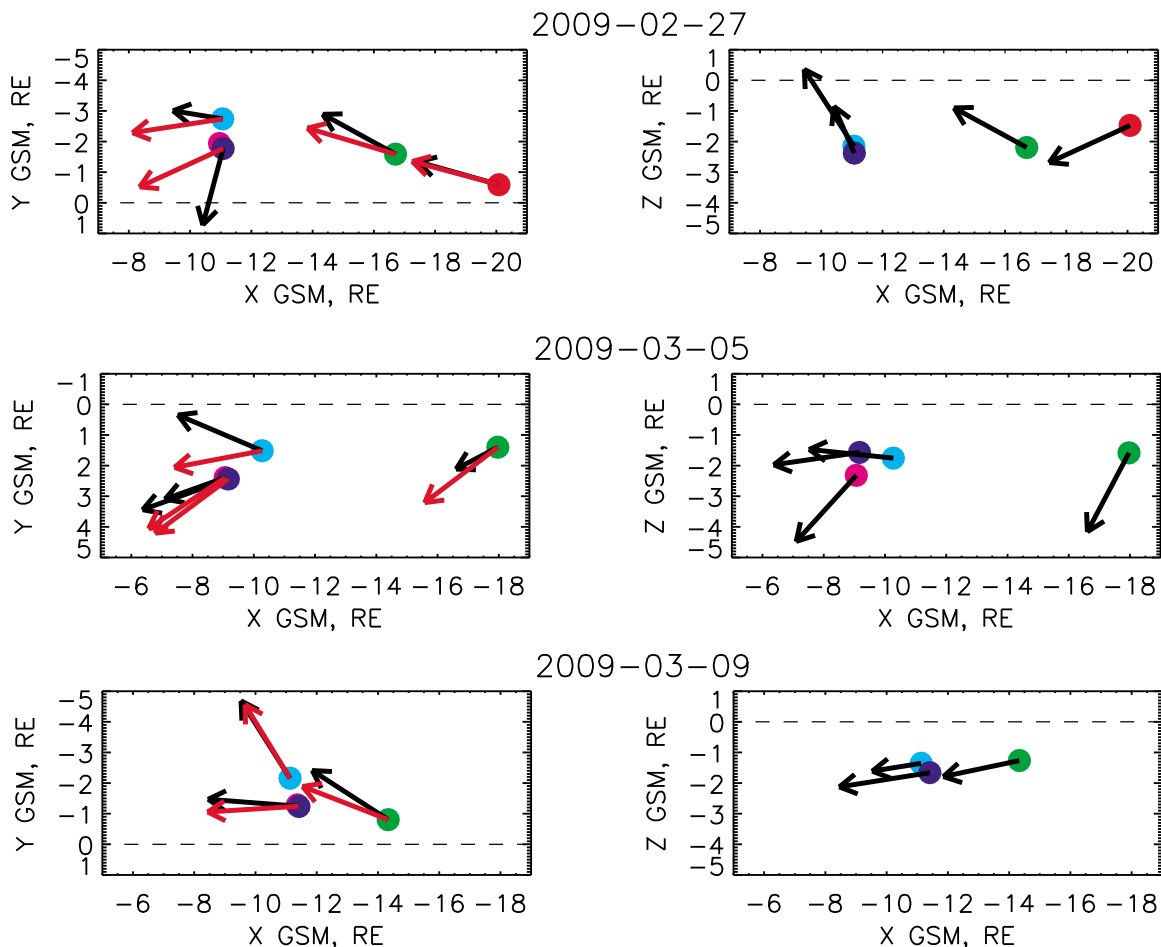
Figure 3. (left) *XY* GSM projections of the MVA-based normals to the fronts (black arrows) and bulk velocity vectors (red arrows) at the corresponding probes for the 27 February, 5 March, and 9 March 2009 events. (right) *XZ* GSM projections of the MVA-based normals for these events.

February 2009 event when THB-THC timing was used too, and the 31 March 2009 event when only THD-THC timing was used). The V_t estimates are listed in Tables 1 and 2.

[12] To investigate front orientations, the minimum variance analysis of the magnetic field (MVAB) [*Sonnerup and Scheible*, 1998] was applied. To define maximum (**L**) and minimum (**N**) variance directions unambiguously, L_z and N_x were set to be positive (northward and earthward, respectively). The MVAB results are summarized in Figures 3 and 4 and in Tables 1 and 2. Resulting MVAB eigenvalues ratios ($\lambda_1 \gg \lambda_2, \lambda_3, \lambda_2/\lambda_3 \sim 10$) indicate that the fronts are locally one-dimensional (1-D) with well defined minimum variation directions. The minimum variance eigenvectors listed in Tables 1 and 2 may be interpreted as front normal vectors. The only exception is the event at THC on 5 March 2009, for which $\lambda_1/\lambda_2 \approx 3$. In this case, THC (the most tailward probe) detected a smoother variation in B_z than those detected by the three other probes located $\approx 8\ R_E$ earthward. This indicates that the front was not fully developed at X = $-18\ R_E$ and steepened while moving inward (see *Li et al.* [2011] for the event description).

[13] Figures 3 and 4 show projections of the front normal vectors onto the *XY* (left column) and *XZ* GSM planes. The left columns also show *XY* projections of the ion bulk velocity, averaged over 3 consecutive spins, centered on the spin containing the corresponding t_0. The results indicate that at X < $-14\ R_E$ the normal and velocity vectors are collinear, and normals at two probes (27 February 2009 THB and THC) separated by $4\ R_E$ are consistent. Closer inward, normal directions at points separated by $1\ R_E$ or fewer along *Y* often disagree. The velocity and front normal vectors often are not collinear deeper in the near-Earth plasma sheet. The 19 March 2009 event shows an earthward moving front with the velocity directed differently at THC, THD, and THE, which were situated at the same *Z*, but separated along *X* and *Y*. The velocity vectors at those points show dawnward rotation, i.e., a vortex structure, similar to that discussed by *Keiling et al.* [2009] and *Panov et al.* [2010]. The observations also show that dawnward probes often detected negative V_y, whereas duskward probes, detected positive V_y. This is consistent with the previous observations of localized plasma-depleted flux tubes in the magnetotail [*Sergeev et al.*, 1996].

[14] To retrieve a common pattern of physical parameter variations during a dipolarization front crossing, we performed a superposed epoch analysis of the observations [*Ohtani et al.*, 2004; *Slavin et al.*, 2003]. Unlike *Ohtani et al.* [2004], we are interested in variations between sec-
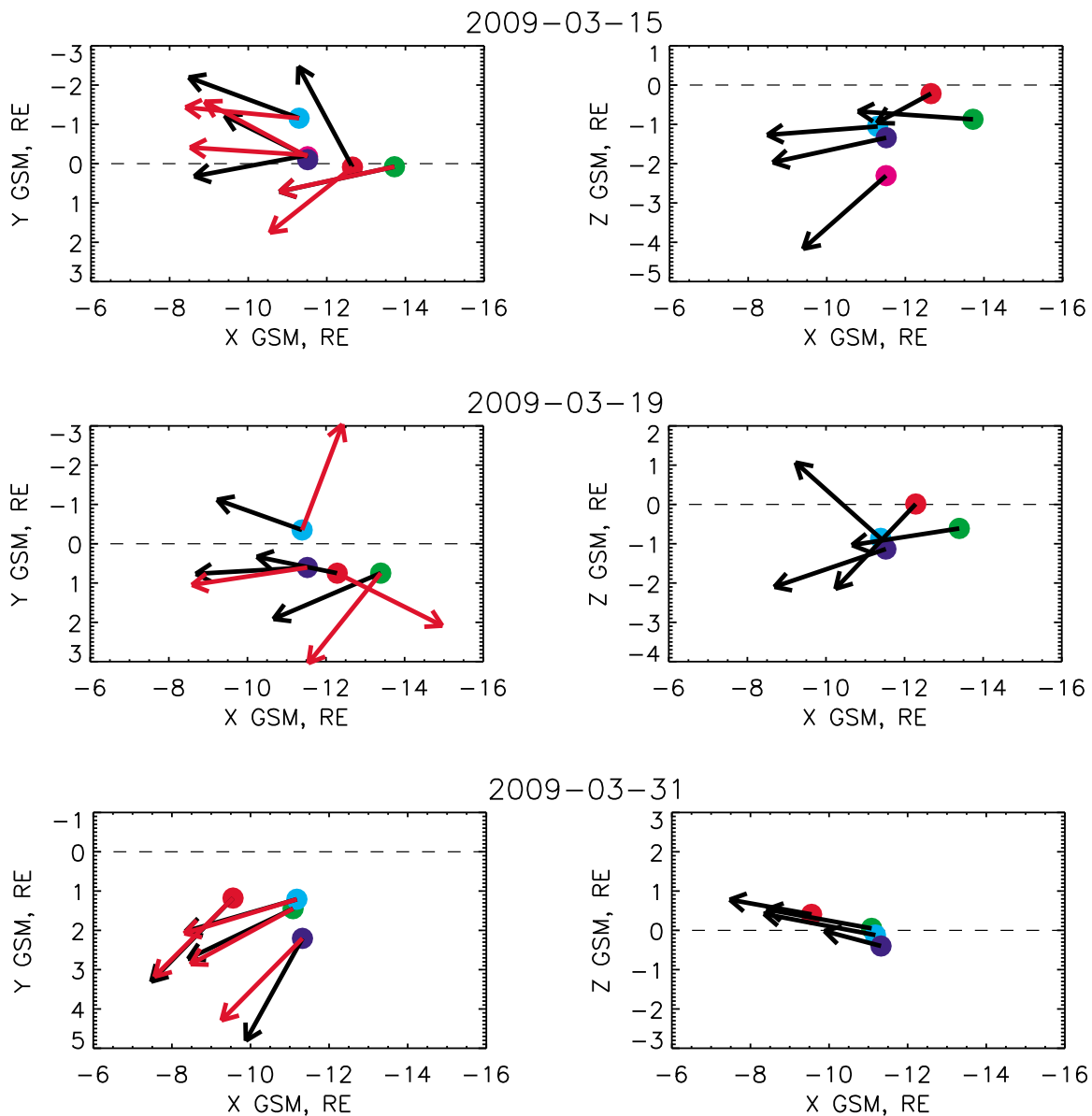
Figure 4. Same as in Figure 3 but for 15, 19, and 31 March 2009 events.

onds and a minute. Figure 5 shows variations in magnetic and electric fields and plasma parameters within ±60 s of t_0 indicating onset of the positive B_z variation (as listed in Tables 1 and 2). A variation is defined as $\delta\xi = \xi(t) - \xi(t_b)$, where $t_b = -60$ s is the start time, and ξ is the physical parameter. Variations in ion and electron energy fluxes (δJ_i and δJ_e), plasma density (δN), and temperature (δT) were normalized by the corresponding values at t_b. These curves show variations in fractions of the corresponding initial values. The median, upper and lower quartiles, calculated from 24 available crossings in 0.25 s windows for the fields (B_z and E_y) and 3 s windows for the plasma parameters, are shown.

[15] The superposed epoch analysis shows that the asymmetric bipolar structure (with amplitudes of negative and positive variation of 3 and 15 nT, respectively) is typically crossed by a probe within 40–50 s (Figure 5a). Behind

it, B_z returns to its undisturbed value $B_z(t_b)$. The cross-tail electric field (E_y) increases to 4–10 mV/m along with the transient B_z increase (Figure 5b), indicating a high rate of magnetic flux transport [*Angelopoulos et al.*, 1992; *Schödel et al.*, 2001], and returns to a background level along with the B_z decay. The ion energy flux, integrated over the SST energy range, increases gradually by a factor of 7, starting at $t \approx -30$ s (Figure 5c). The >10 keV electron energy flux shows a step-like increase at t_0 (Figure 5d). Although a large difference between lower and upper quartiles indicates different behavior of the energetic electron flux event by event, median value shows an increase by factor of 3, i.e., significantly less than that for ions. The upper quartile, however, shows much stronger energization (up to factor of 15) in some cases. The plasma concentration first gradually increases ahead of the front, starting at $t \approx -40$ s, and then rapidly decreases at the front to ~0.5 of the initial value
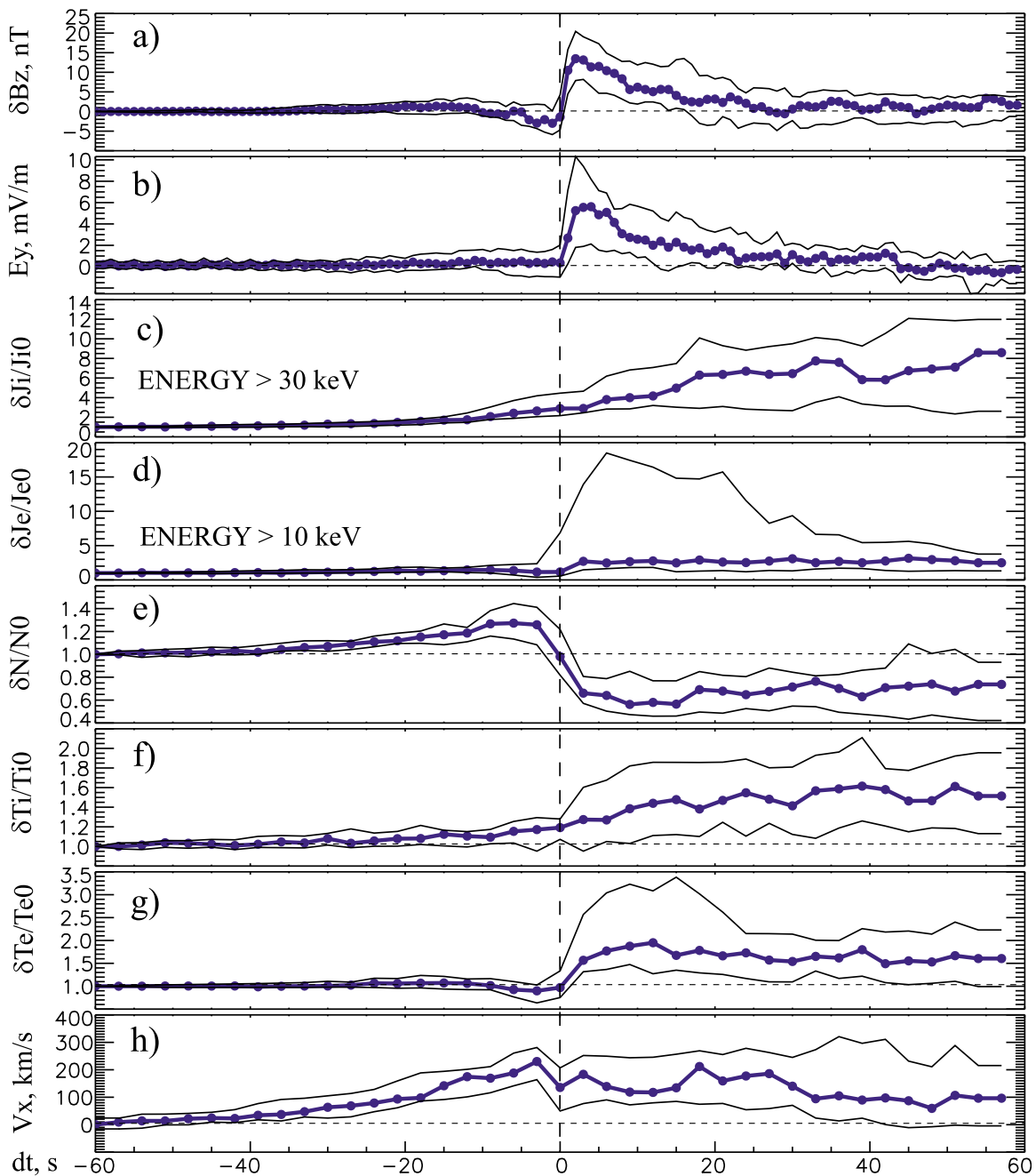
Figure 5. Superposed epoch analysis of magnetic field and particle observations. Median (thick blue lines) and lower and upper quartiles (thin black lines) of (a) B_z variations (δB_z), (b) cross-tail electric field (E_y), (c) ion and (d) electron integrated energy fluxes, normalized by the initial value ($\delta J_i/J_{i0}$, $\delta J_e/J_{e0}$), (e) normalized density ($\delta N/N_0$), (f) ion ($\delta Ti/T_0$) and (g) electron ($\delta T_e/T_0$) variations, and (h) X component of ion velocity. Here t_0 (vertical dashed line) indicates onset of the positive B_z variation. GSM coordinate system is used.

(Figure 5e). Interestingly, although B_z returns to its initial value behind the dipolarization, the median density stays at ≈ 0.5 N_0 during at least a minute after front onset ($dt = 0$). Starting at $t \approx -40$ s, ion temperature increases gradually to a factor of 1.6 and stays at this level behind the front ($dt > 0$, Figure 5f). The median electron temperature shows a small decrease coinciding with the negative B_z variation and a

rapid increase in factor of 2 at the front (Figure 5g). It stays at this level at $t > 0$. The $\delta T_e/T_{e0}$ upper quartile exhibits a transient ≈ 20 s long increase with maximum of 3, indicating intensive heating of electrons at the front in some cases. V_x increases gradually to ≈ 200 km/s in average, starting at $t \approx -40$ s (Figure 5h). Since the enhancement of V_x at $t < 0$ does not correspond to an increase in E_y, the plasma flow ahead
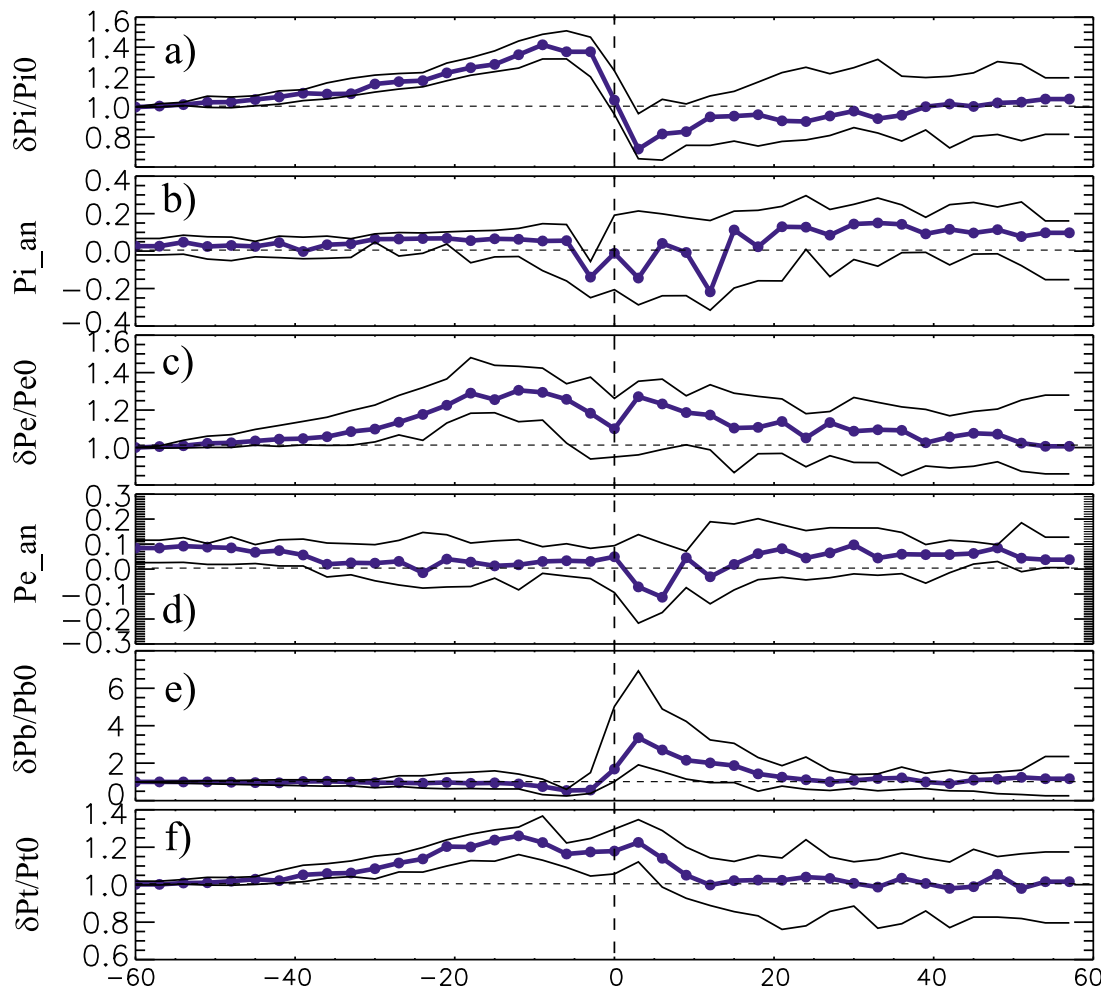
Figure 6. Superimposed epoch analysis of (a) normalized ion pressure variations ($\delta P_i/P_{i_0}$), (b) ion pressure anisotropy ($P_{ian} = (P_\parallel - P_\perp)/P_\parallel$, (c) normalized electron pressure variations ($\delta P_e/P_{e0}$),(d) electron pressure anisotropy (P_{ean}), (e) normalized magnetic pressure variations ($\delta P_b/P_{b0}$), and (f) normalized total pressure variations ($\delta P_t/P_{t0}$). Here t_0 (vertical dashed line) indicates onset of the positive B_z variation. Median (thick blue lines) and lower and upper quartiles (thin black lines) are shown.

of the front does not transport significant magnetic flux. The median value of V_x stays approximately constant behind the front, although difference between upper and lower quartiles indicates significant variations in the data. It should be noted that in individual events, V_x was reported to achieve larger values (500–800 km/s [see *Runov et al.*, 2009; *Sergeev et al.*, 2009; *Li et al.*, 2011]).

[16]   Results shown in Figure 5 resemble those of *Ohtani et al.* [2004] (see their Figure 4), which were obtained within larger time window (±10 min): the asymmetric bipolar variation in B_z with a small-amplitude negative dip preceding a large-amplitude positive jump is associated with a pronounced drop in plasma number density (note a linear scale in Figure 4 of *Ohtani et al.* [2004]) and more gradual increases in ion temperature and bulk velocity. According to *Ohtani et al.*'s [2004] results, the $V_\perp$ onset preceded the positive δB_z one by ≈2 min; the δB_z amplitude was ≈7 nT in average (versus our 15 nT). These differences are, mainly, due to our selection criteria, setting the minimum

δB_z = 10 nT within δt < 30 s. Note also the smaller sampling rate data (12 s), used by *Ohtani et al.* [2004].

[17]   Our results are also similar to those obtained statistically by *Slavin et al.* [2003] with Geotail data. *Slavin et al.* [2003] showed density and bulk velocity increases 40–60 s ahead of the asymmetric bipolar variation in B_z, interpreted as a flux rope signature. We will return to this point in section 4.

[18]   Figure 6 shows normalized variations in ion, electron, magnetic, and total pressures and ion and electron pressure anisotropies during dipolarization front crossings. The ion pressure (Figure 6a) exhibits a positive variation ahead of the front, staring at $t \approx -40$ s, in accord with pressure and temperature variations. The median ion pressure decreases rapidly down to ≈0.7 of the initial value at the front and gradually increases up to the initial value for ≈40 s after front crossing. The ion pressure decrease behind the front is caused by the rapid density decrease, which is not compensated by the gradual increase in the ion temperature. The superimposed epoch analysis results suggest a
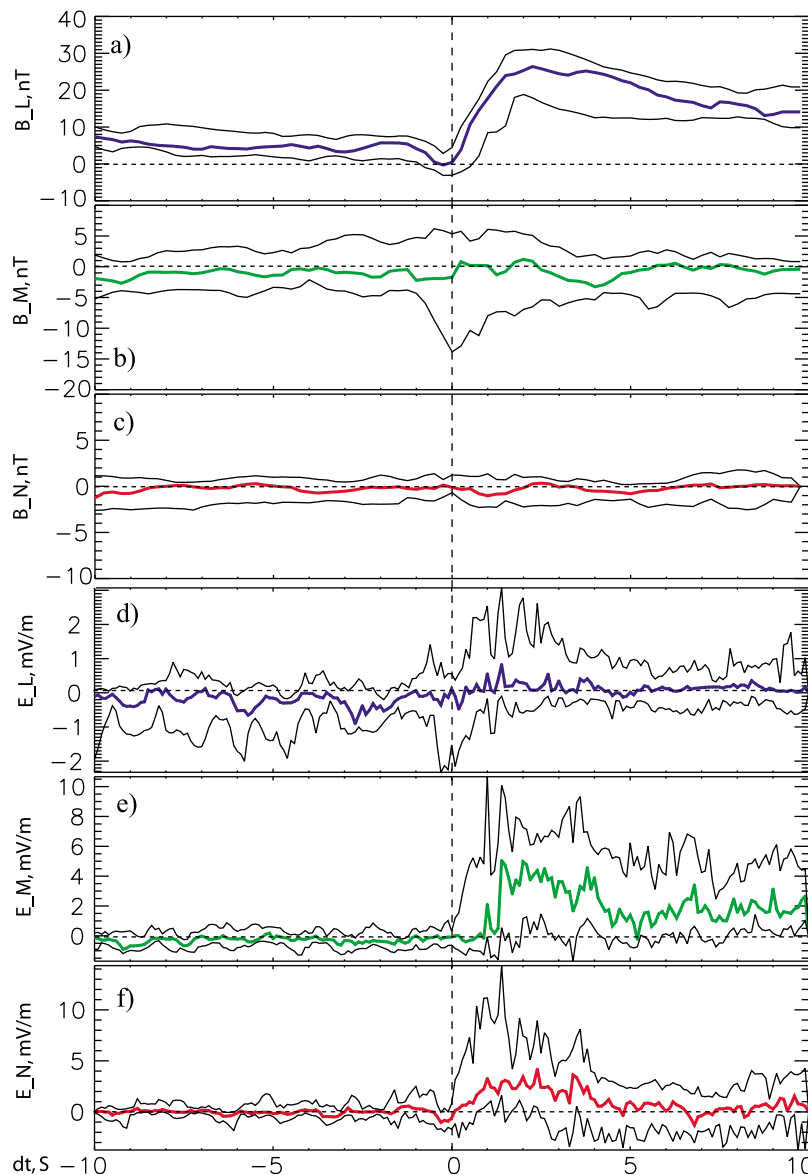
Figure 7. Superimposed epoch analysis of (a–c) magnetic and (d–f) electric $\mathbf{E}' = \mathbf{E} + \mathbf{V}_i \times \mathbf{B}$ field observations. Median (thick lines) and upper and lower quartiles are shown. The MVAB coordinate system is used. Data within interval ±10 s with respect to the dipolarization front onset (t_0) are plotted.

minor (≤20%) negative anisotropy ($P_{i\perp} > P_{ipar}$) within $-5 < t < 15$ s (Figure 6b). The electron pressure also increases ahead of the front, then relaxes gradually to the initial value (Figure 6c). Evidently, the electron temperature, rapidly increasing behind the front, compensates or even overcomes the drop in the density. The median value of the electron pressure anisotropy exhibits a small (≤10%) negative variation within ≈15 s around the front (Figure 6d). The magnetic pressure $P_b = B^2/(2\mu_0)$ increases at the front by a factor of 3 (the median value) and returns to approximately initial value within ≈30 s behind the front (Figure 6e). The median total pressure $P_t = P_b + P_i + P_e$ increases ahead of the front in accord with the ion pressure, stays at the increased level behind the front ($0 < t < 10$ s) due to the

increase in P_b there, and relaxes to the initial value afterward (Figure 6f).

[19] To study front-related patterns in magnetic and electric fields, a superposed epoch analysis of the magnetic and electric fields in variance directions (MVAB) was applied. The results are shown in Figure 7. The magnetic field shows strong variations in only the maximum variance component (L, Figure 7a) which is close to Z GSM for all cases. To analyze the electric field observations, we calculate the spin axis component of the field using the $\mathbf{E} \cdot \mathbf{B} = 0$ approximation and add $\mathbf{V}_i \times \mathbf{B}$, where $\mathbf{V}_i$ and $\mathbf{B}$ are the ion velocity calculated from ESA and SST measurements and magnetic field, respectively, interpolated to the $\mathbf{E}$ field cadence. The derived electric field vector $\mathbf{E}' = \mathbf{E} + \mathbf{V}_i \times \mathbf{B}$
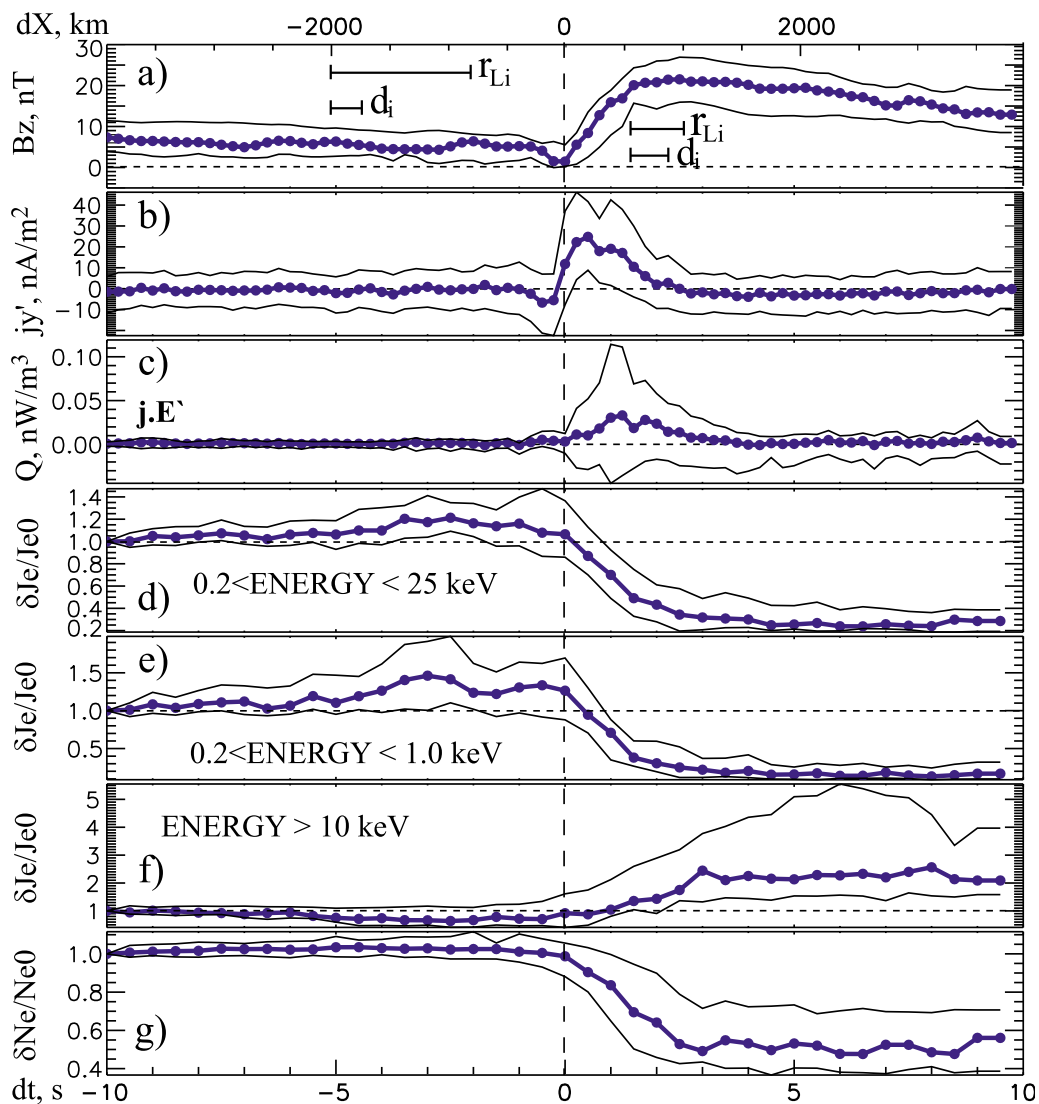
Figure 8. Superimposed epoch analysis of (a) B_z, (b) a current density $j'_y = \mu_0^{-1}\Delta B_z/\Delta X$, (c) Joule heating rate $Q = j' E'_M$, (d–f) integrated electron flux with 3/16 s sampling rate (see text for details), and (g) electron number density, estimated from spacecraft potential data (1/8 s sampling rate). The upper axis shows the spatial scale ΔX in kilometers (see text for details). Seventeen out of twenty-four events are used. The horizontal bars show median ion thermal gyroradii (R_{Li}) and ion inertial length (d_i) ahead and behind the front.

was rotated into the MVAB system. The results show no pattern in E_L (Figure 7d), and clear patterns in the E_M and E_N components (Figures 7e and 7f, respectively). In the MVAB system, the intermediate variance component (E_M) was set to be duskward (note that LMN is left-handed system). E_M shows an increase at (or slightly after) the front up to ≈5 mV/m (median) and 8 mV/m (upper quartile). This E_M enhancement lasts about 5 s. E_M decreases to ≈2 mV/m (median) afterward. The normal component of the electric field (E_N) shows a rather gradual increase at the front to ≈3 mV/m in median value. It also lasts about 5 s. The E_N upper quartile shows a maximum of 10 mV/m at the front.

[20] Estimation of front propagation velocity (V_t) by timing of front arrivals makes it possible to estimate the scale of the front and reconstruct a profile of the current density component $j'_y = -\mu_0^{-1}\partial Bz/\partial X \sim \Delta Bz/\Delta X$, where $\Delta X = X_0 - \int_{t_b}^{t_e} V_t dt$, $X_0 = 0$ at $t = t_0$ [*Runov et al.*, 2011]. Assuming gyrotropy of electrons, the electron flux may be calculated with a 3/16 s time resolution using the flux at each subsequent angular sector [*Sergeev et al.*, 2009; *Zhang et al.*, 2011]. This gives us an opportunity to reconstruct electron flux changes within the front. Finally, the electron density may be estimated from the spacecraft potential measured by EFI [*Mozer*, 1973]. These methods allowed us to reconstruct the spatial structure of the dipolarization front, presented in Figure 8. Only events with front normals close to X direction in the XY plane (atan(N_y/N_x) < 45°) were used for the reconstruction. The 5 March 2009 THC event showing the underdeveloped front

was excluded as well. The reconstructed median scale of the dipolarization front (from a local minimum to a maximum) was found to be 500–700 km. The current density j'_y (Figure 8b) increases at the front to 20 nT/m^2 (median), which is a factor of 5–7 larger than the "equatorial" part of j_y ($j_{y0} = \mu_0\ \partial B_x/\partial Z$), estimated using magnetic field measurements at probes THE and THA, which were situated at the same X and Y and separated along Z by about 1 R_E (see Figures 1 and 2). This is in agreement with results from event studies [*Runov et al.*, 2011; *Zhang et al.*, 2011]. The energy conversion rate in the reference frame moving with the ions $Q = \mathbf{j} \cdot \mathbf{E}' \approx j'_y E'_M$ (Figure 8c) is, on average, positive with a peak of 0.05 nW/m^3 (up to 0.1 nW/m^3 in the upper quartile), indicating dissipation, i.e., magnetic field-to-plasma energy conversion. The lower quartile of Q, however, is negative with a peak of -0.04 nW/m^3, indicating a possibility of dynamo (plasma-to-field energy conversion) for some events. The energy conversion rises within 3–4 s at the front, i.e., in ≈1000 km thick layer. The integrated electron flux (J_e) at energies $0.2 < E < 25$ keV (Figure 8d) decreases to ≈0.4 of the initial value within the boundary layer with a thickness of 1000 km, while J_e at energies $E > 10$ keV increases to a factor of 2 within this layer (Figure 8g). The increase in electron flux ahead of the front is most pronounced for the low-energy population ($0.2 < E < 1$ keV, Figure 8e). The flux of high-energy electrons decreases ahead of the front. In agreement with the low-energy electron flux, the electron density estimated from the spacecraft potential decreases to about one half the initial value within the 1000 km thick boundary layer. To give a reader an idea of physical scales, the median values of ion thermal gyroradii ahead and behind the front (1200 and 600 km, respectively) and ion inertial length ahead and behind the front (320 and 440 km, respectively) are shown in Figure 8a by horizontal bars.

4. Discussion and Summary

[21] We have studied properties of inward moving dipolarization fronts with 6 selected events (24 individual front crossings). The selection criteria, which dramatically reduced the number of events, required the front detection by at least 3 probes in a row. The advantage of this selection criterion was to ensure accurate estimation of the front velocity in order to convert time differences to spatial scales. A disadvantage, however, is a statistically small data set. To determine a common pattern in fields and plasma parameters during front crossings, we performed a superposed epoch analysis of the observations using ±60 s and ±10 s time windows around B_z positive variation onset. The analysis reveals clear patterns, as follows.

[22] 1. The northward component of the magnetic field (B_z) shows a strongly asymmetric bipolar variation with the negative part amplitude factor of 3 smaller than that of the positive part (Figure 5). A typical duration of the entire variation is 40–50 s. With front velocities varying between 200 and 500 km/s (see Tables 1 and 2), a typical scale size of the entire structure is 2–3 R_E. The thickness of the dipolarization front (i.e., the positive variation from local minimum to maximum) is 500–1000 km.

[23] 2. Dawn-dusk and front normal electric field components in average, increase at the front to 5 and 3 mV/m, respectively. In some events, the electric field increase exceeded 10 mV/m (see Figure 7). The typical duration of the normal electric field enhancement is 3–5 s, which corresponds to a scale size of 1000 km. The enhancement in the dawn-dusk component may last longer (10 to 40 s).

[24] 3. In the particle number density, an increase up to 1.2 of the initial value followed by a rapid decrease to 0.5 of the initial value were observed at the front in all selected cases. The temporal and spatial scales of the density decrease are 2–3 s and 500–1000 km, respectively. The gradual increase in the ion temperature does not compensate the drop in density, which results in an ion pressure decrease behind the front.

[25] 4. Increases in high-energy (>10 keV) electron flux and, correspondingly, in the electron temperature were observed within 3 s behind the front. The electron temperature increase compensates for or even prevails the density drop. Therefore, the electron pressure, contrary to the ion one, increases behind the front (see Figure 6).

[26] Our results show that flux of high-energy ions and ion temperature increase around the front only gradually, showing, contrary to electron flux and temperature, no abrupt increase at the front. This may be explained by (1) a compression of ambient plasma ahead of the dipolarization front [*Li et al.*, 2011] and (2) the remote sensing of the approaching front by high-energy ions [*Zhou et al.*, 2010]. The ion velocity increase prior to the step-like (or spike-like) increase in B_z was also shown in hybrid simulations of reconnection-related dipolarization [*Hesse et al.*, 1998].

[27] Results of magnetic field MVA (Figures 7a–7c) and observations of the 10 keV electron flux increase behind the front (Figures 5d and 8f) agree with the results obtained by *Sormakov and Sergeev* [2008] showing that the asymmetric bipolar variation in B_z is more consistent with NFTE-like structures than with flux ropes. Analyzing cases with negative variations ($B_L < -0.1$ nT), we found 2 of total 8 cases in the close proximity to the neutral sheet ($|B_x| < 3$ nT). The other 6 were observed at $|B_x|$ level varying between 6 and 12 nT. Thus, the NFTE-like geometry is more probable for dipolarization front, however, the magnetic structure around the front may include small-scale magnetic islands, similar to the secondary islands, reported in some observations of magnetic reconnection in the magnetotail [*Nakamura et al.*, 2006; *Eastwood et al.*, 2007] and in particle-in-cell (PIC) simulations [e.g., *Divin et al.*, 2007]. Figure 9a illustrates the magnetic field geometry in the vicinity of the dipolarization front, showing the magnetic field lines resulting from PIC simulations of transient reconnection [*Sitnov et al.*, 2009]. The similar structures with a small amplitude $\delta B_z < 0$ preceding a large-amplitude $\delta B_z > 0$ are also pronounced in hybrid [see, e.g., *Krauss-Varban and Karimabadi*, 2003, Figure 1] and, although larger in scales, in MHD simulations [see, e.g., *Birn and Hesse*, 2000, Plate 3; *Wiltberger et al.*, 2000, Figure 8]. It is worth noting that B_z returns to its initial (undisturbed) value ($\delta B_z \approx 0$) after bipolar structure passage. The lower quartile of δB_z is negative. These signatures indicate current sheet restoration behind the passing bipolar magnetic structure, which agrees with the MHD model of transient reconnection [*Semenov et al.*, 2005;
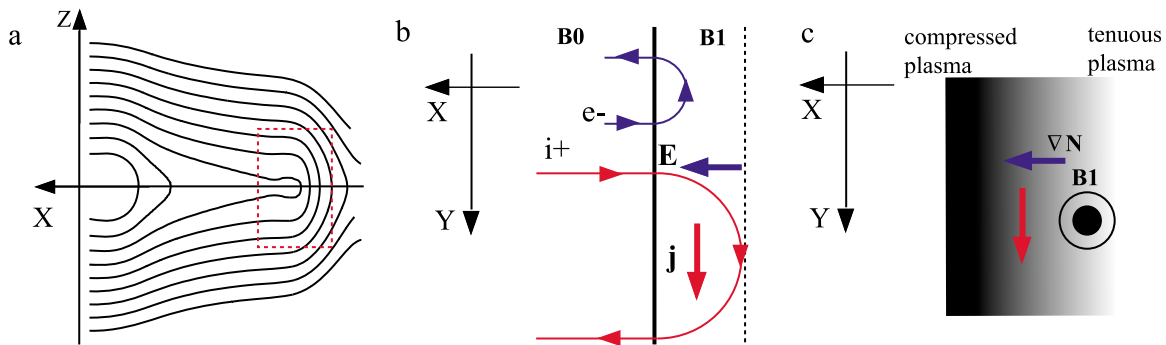
Figure 9. Geometry and structure of a dipolarization front. (a) Magnetic field configuration in the *XZ* plane (magnetic field lines resulting from PIC simulations by *Sitnov et al.* [2009]; a dashed-line box shows the front region). (b) The dipolarization front as a "magnetopause"; schematic ion and electron trajectories in the front proximity, and resulting electric field (blue arrow) and current (red arrow). (c) A schematic of the ∇N -driven current formation (plasma density is gray scale coded).

Kiehas et al., 2009]. Thus, it appears that the mechanism forming the bipolar magnetic structure is not kinetic and may be described using the MHD approach.

[28] Kinetic effects become important in the boundary layer where magnetic field, electron fluxes, and density experience dramatic changes (see Figure 8). The characteristic scale of magnetic field, electron fluxes and plasma density gradients is estimated to be of 500–1000 km, which is comparable with the ion thermal gyroradius. Our analysis at this point confirms results of previous event studies [*Runov et al.*, 2009, 2011; *Sergeev et al.*, 2009]. The B_z gradient along X is, in average, 5–10 times larger than B_x gradient along Z. The MVA normals to the fronts (Tables 1 and 2, Figures 3 and 4) are well defined and lay mainly in the *XY* plane. Thus, the dipolarization front is a vertical current sheet with the current density $j_y \approx -\mu_0^{-1} \partial B_z/\partial X$ and thickness of the ion thermal gyroradius. Since the probe, situated 1 R_E southward of the neutral sheet often did not detect the sharp B_z increase, this current sheet seems to be localized in Z direction within 1–2 R_E.

[29] Being a thin boundary, a vertical current sheet, separating two distinct plasma populations, the dipolarization front may be described as a magnetopause of the energetic plasma intrusion into the quiet plasma sheet. The analogy with the magnetopause is helpful to understand the kinetic thickness of the front. Let us consider the front as sharp boundary separating regions with $\mathbf{B}_0$ and $\mathbf{B}_1$, where $\mathbf{B} = \{0 ,0, B_z\}$, $\mathbf{B}_1 \gg \mathbf{B}_0$, moving with respect to the ambient plasma. In the frame of reference moving with the front, particles of the ambient plasma sheet hit the front and perform, in ideal case, half a gyration in the enhanced magnetic field. The different gyromotion of ions and electrons will result in an electric current in the Y direction. Figure 9c schematically depicts the situation [see also *Baumjohann and Treumann*, 1996, p. 191 and Figure 8.16]. The thickness of the resulting current sheet is of the order of average thermal gyroradius in the magnetic field B_{z1}. For $B = 15$ nT and ion temperature 5 keV, the sheet thickness is ≈ 700 km which is consistent with the observations. The difference in ion and electron gyroradii leads to charge separation in this current sheet resulting in the electric

field, directed earthward along the front normal. Observations indeed have shown E_N enhancement at and behind the front (see Figure 7). A comparison between the average normal electric field (E_N) and the Hall electric field $E_h = \mathbf{j} \times \mathbf{B}/ne \approx j_yBz/ne$, estimated using median values of B_z, j'_y, and the electron density, shows good agreement at the front ($-1 < dt < 2$ s). E_N and E_h disagree behind the front (Figure 10, right). Our analysis, therefore, supports the previous results by *Zhou et al.* [2009] only partially.

[30] The strong plasma density gradient at the front suggests another current component in the front current sheet: the diamagnetic current $\mathbf{j_d} = \mathbf{B}/\mathbf{B}^2 \times \nabla_\perp \mathbf{P}_\perp$. Since the ion pressure decreases rapidly at the front and the electron pressure, on average, does not exhibit sharp changes (see Figure 6), the main contribution to the current for the events studied herein is the ion pressure gradient drift. In our idealized geometry, assuming front planarity and taking into account the gradual increase in T_i (see Figure 5), $j_{d_y} = B_z/B^2\partial P/\partial X \approx B_z/B^2 T_i \partial N/\partial X$. Because the density gradient is directed along positive X (earthward), the resulting current flows along positive Y (duskward). Assuming that fronts move with approximately constant velocities V_t with respect to the probes, a linear correlation between $\partial B_z/\partial t$ and $\partial n/\partial t$ is expected. Such a correlation is shown in Figure 10. Figure 9c presents a schematic view of the j_{d_y} formation on the dipolarization front. It is worth noting that our conclusions are based on variations in the pressure median value derived from the 6 selected events. In some cases, such as the case studied by *Zhang et al.* [2011], the electron pressure may decrease at the front, and the current due to $\nabla_\perp P_e$ may dominate.

[31] Enhancement of the duskward electric field component of $\mathbf{E}'$ is likely due to a difference in electron and ion velocities at the front, resulting in a difference between $-V_{ix}B_z$ and $-V_{ex}B_z$ [*Sitnov et al.*, 2009]. A caution is needed, however: underestimation of ion velocity cannot be ruled out. $Q = \mathbf{j} \cdot \mathbf{E}' > 0$ indicates Joule heating at the front (Figure 8). Thus, the fronts are earthward moving dissipation regions where electromagnetic energy is converted to thermal energy of plasma (particle kinetic energy). Assuming a scale size of 1000 km, the Joule heating rate in the front current sheet
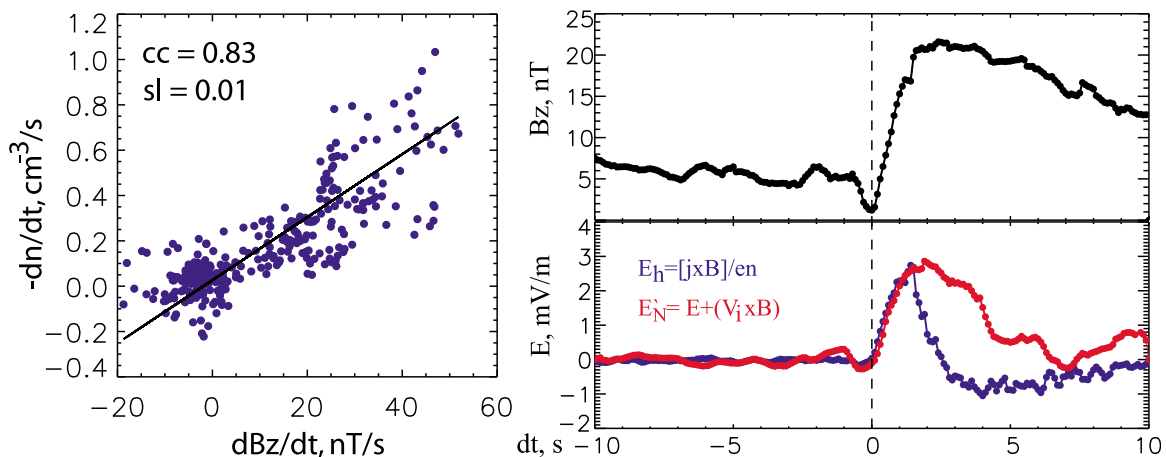
Figure 10. (left) Correlation analysis of magnetic field ($\partial B_z/\partial t$) and plasma density ($-\partial n/\partial t$) change rates. (right) A comparison between median values of the observed normal electric field (E'_N) and the estimated Hall electric field (E_h). Top right panel shows median B_z.

reaches ~0.1 mW/m^2 or ~0.1 erg/s/cm^2 ~10^{16} erg/s/R_E^2. Thus, Joule heating at the dipolarization front may provide ~10% of the total BBF power [*Angelopoulos et al.*, 1996, 1997]. Enhancement of Joule heating at dipolarizations was also shown in PIC simulations of reconnection [*Sitnov et al.*, 2009; *Pritchett*, 2010]. In these simulations, the dissipation at the front is strongly dominated by ions ($j_{i_y}E_y \gg j_{e_y}E_y$). Our studies suggest that because of $\nabla_\perp P_i > \nabla_\perp P_e$, the ion contribution to the current and therefore to the dissipation at the front may indeed be dominant. It is worth noting that the high dissipation rate assumes significant changes in fields and particle fluxes as the front progresses earthward. Quantitative analysis of these changes will be done in future studies.

[32] Dipolarization fronts, which are associated with rapid increase in high-energy particle fluxes and enhancement in the electric field, may be considered as earthward moving injection boundaries [e.g., *Moore et al.*, 1981]. Our results indicate that electric field enhancement is spatially localized in a layer with thickness comparable to the inward propagating ion thermal gyroradius, which may survive for ~100 s. Thus, E_M enhancement at and behind the front (Figure 7) provides the azimuthal electric field pulse assumed in modeling of dispersionless injections [*Li et al.*, 1998, 2003]. Acceleration of particles by the enhanced electric field at transient dipolarizations was studied by *Birn et al.* [1997a, 1997b, 2004]. They traced test particles through the fields, resulting from generic MHD simulations. The regions of the enhanced electric field were, however, on a scale of several R_E. A question on particle energization at gyroscale dipolarization fronts is still open. A simple model of ion energization in thin sheet with enhanced B_z and E_y, assuming an acceleration mechanism, similar to that in the quasi-parallel bow shock, results with the ion spectrum similar to that observed ahead of dipolarization fronts [*Zhou et al.*, 2010]. Detailed analysis of observed distribution functions and comparison with results of self-consistent kinetic simulations are needed to understand processes of particle energization at dipolarization fronts.

[33] A density gradient with a scale comparable to the ion gyroradius is a favorable condition for drift mode wave excitation and development of drift instabilities. Wave activity at low hybrid frequency at the front was indeed observed in case studies [*Sergeev et al.*, 2009; *Zhou et al.*, 2009].

[34] The analysis of the dipolarization front orientation reveals large differences in front normal directions at probes separated azimuthally by ≈ 1 R_E (Figures 3 and 4). Such a short correlation length may indicate that the edge of the energetic plasma intrusion is interchange unstable [*Nakamura et al.*, 2002a; *Pritchett and Coroniti*, 2010; *Guzdar et al.*, 2010]. Although transient magnetic reconnection is most plausible mechanism to generate high-energy plasma jets with reduced density carrying the enhanced northward (southward) magnetic field (B_z), often in a form of the quasi-bipolar variation [*Semenov et al.*, 2005; *Sitnov et al.*, 2009], the kinetic interchange instability of such magnetic configuration may lead its steepening along X and structuring along Y [*Pritchett and Coroniti*, 2010]. The 5 March 2009 event shows an example of this scenario (Figure 1): THC at $X = -18$ R_E detected a relatively smooth B_z variation embedded into fast flow (see *Li et al.* [2011] for details), while the three innermost probes detected the well-formed front. Interestingly, THD and THE detected another front, following the first one. A similar event was reported by *Zhou et al.* [2009]. These recurrent fronts may be formed by individual pulses of reconnection, or result from crossing adjacent "fingers" of the interchange unstable boundary of the hot plasma intrusion.

[35] To conclude, we used THEMIS multiprobe observations to find the standard patterns in fields and particle parameter variations during crossings of the dipolarization fronts. The one-dimensional profile of the front was reconstructed assuming its earthward propagation at a constant velocity. Multipoint measurements with smaller separations along all three directions are needed to resolve the fine structure of dipolarization fronts and related particle

dynamics. These topics are to be addressed to future studies of THEMIS observations during 2010 and 2011 tail seasons and to future multispacecraft magnetospheric missions, such as MMS.

References

Angelopoulos, V. (2008), The THEMIS mission, *Space Sci. Rev.*, *141*, 5–34.

Angelopoulos, V., W. Baumjohann, C. F. Kennel, F. V. Coroniti, M. G. Kivelson, R. Pellat, R. J. Walker, H. Lühr, and G. Paschmann (1992), Bursty bulk flows in the inner central plasma sheet, *J. Geophys. Res.*, *97*, 4027–4039.

Angelopoulos, V., et al. (1994), Statistical characteristics of bursty bulk flow events, *J. Geophys. Res.*, *99*, 21,257–21,280.

Angelopoulos, V., et al. (1996), Multipoint analysis of a bursty bulk flow event on April 11, 1985, *J. Geophys. Res.*, *101*, 4967–4989.

Angelopoulos, V., et al. (1997), Correction to "Multipoint analysis of a bursty bulk flow event on April 11, 1985" by V. Angelopoulos et al., *J. Geophys. Res.*, *102*, 211–212.

Auster, H. U., et al. (2008), The THEMIS fluxgate magnetometer, *Space Sci. Rev.*, *141*, 235–264.

Baumjohann, W., and R. A. Treumann (1996), *Basic Space Plasma Physics*, 329 pp., Imperial Coll. Press, London.

Birn, J., and M. Hesse (2000), The current disruption myth, in *Magnetospheric Current Systems*, edited by S.-I. Ohtani et al., pp. 285–294, AGU, Washington, D. C.

Birn, J., M. F. Thomsen, J. E. Borovsky, G. D. Reeves, D. J. McComas, R. D. Belian, and M. Hesse (1997a), Substorm ion injections: Geosynchronous observations and test particle orbits in three-dimensional dynamic MHD fields, *J. Geophys. Res.*, *102*, 2325–2341.

Birn, J., M. F. Thomsen, J. E. Borovsky, G. D. Reeves, D. J. McComas, R. D. Belian, and M. Hesse (1997b), Substorm electron injections: Geosynchronous observations and test particle simulations, *J. Geophys. Res.*, *102*, 2325–2341.

Birn, J., M. Thomsen, and M. Hesse (2004), Electron acceleration in the dynamic magnetotail: Test particle orbits in three-dimensional magnetohydrodynamic simulation fields, *Phys. Plasmas*, *11*, 1825–1833.

Bonnell, J. W., F. S. Mozer, G. T. Delory, A. J. Hull, R. E. Ergun, C. M. Cully, V. Angelopoulos, and P. R. Harvey (2008), The electric field instrument (EFI) for THEMIS, *Space Sci. Rev.*, *141*, 303–341.

Divin, A. V., M. I. Sitnov, M. Swisdak, and J. F. Drake (2007), Reconnection onset in the magnetotail: Particle simulations with open boundary conditions, *Geophys. Res. Lett.*, *34*, L09109, doi:10.1029/2007GL029292.

Eastwood, J. P., et al. (2007), Multi-point observations of the Hall electromagnetic field and secondary island formation during magnetic reconnection, *J. Geophys. Res.*, *112*, A06235, doi:10.1029/2006JA012158.

Guzdar, P. N., A. B. Hassam, M. Swisdak, and M. I. Sitnov (2010), A simple MHD model for the formation of multiple dipolarization fronts, *Geophys. Res. Lett.*, *37*, L20102, doi:10.1029/2010GL045017.

Hesse, M., J. Birn, and D. Winske (1998), Formation and structure of thin current sheets in the magnetotail: Dipolarization, in *Substorms-4*, edited by S. Kokubun and Y. Kamide, pp. 727–730, Kluwer Acad., Dordrecht, Netherlands.

Keiling, A., et al. (2009), Substorm current wedge driven by plasma flow vortices: THEMIS observations, *J. Geophys. Res.*, *114*, A00C22, doi:10.1029/2009JA014114.

Kiehas, S. A., et al. (2009), First application of a Petschek-type reconnection model with time-varying reconnection rate to THEMIS observations, *J. Geophys. Res.*, *114*, A00C20, doi:10.1029/2008JA013528.

Krauss-Varban, D., and H. Karimabadi (2003), Timing and localization of reconnection signatures—Is there a substorm model problem?, *Geophys. Res. Lett.*, *30*(6), 1308, doi:10.1029/2002GL016369.

Li, S.-S., V. Angelopoulos, A. Runov, X.-Z. Zhou, J. McFadden, D. Larson, J. Bonnell, and U. Auster (2011), On the force balance around dipolarization fronts within bursty bulk flows, *J. Geophys. Res.*, doi:10.1029/2010JA015884, in press.

Li, X., D. N. Baker, M. Temerin, G. D. Reeves, and R. D. Belian (1998), Simulation of dispersionless injections and drift echoes of energetic electrons associated with substorms, *Geophys. Res. Lett.*, *25*, 3763–3766.

Li, X., T. E. Sarris, D. N. Baker, W. K. Peterson, and H. J. Singer (2003), Simulation of energetic particle injections associated with a substorm on August 27, 2001, *Geophys. Res. Lett.*, *30*(1), 1004, doi:10.1029/2002GL015967.

McFadden, J. P., C. W. Carlson, D. Larson, V. Angelopoulos, M. Ludlam, R. Abiad, and B. Elliot (2008), The THEMIS ESA plasma instrument and in-flight calibration, *Space Sci. Rev.*, *141*, 277–302.

Moore, T., R. Arnoldy, J. Feynman, and D. Hardy (1981), Propagating substorm injection fronts, *J. Geophys. Res.*, *86*, 6713–6726.

Mozer, F. S. (1973), Analysis of techniques for measuring DC and AC electric fields in the magnetosphere, *Space Sci. Rev.*, *14*, 272–313.

Nakamura, M. S., H. Matsumoto, and M. Fujimoto (2002a), Interchange instability at the leading part of reconnection jets, *Geophys. Res. Lett.*, *29*(8), 1247, doi:10.1029/2001GL013780.

Nakamura, R., et al. (2002b), Motion of the dipolarization front during a flow burst event observed by Cluster, *Geophys. Res. Lett.*, *29*(20), 1942, doi:10.1029/2002GL015763.

Nakamura, R., et al. (2006), Dynamics of thin current sheets associated with magnetotail reconnection, *J. Geophys. Res.*, *111*, A11206, doi:10.1029/2006JA011706.

Ohtani, S. (1998), Earthward expansion of tail current disruption: Dual-satellite study, *J. Geophys. Res.*, *103*, 6815–6825.

Ohtani, S., K. Takahashi, T. Higuchi, A. T. Y. Lui, H. E. Spence, and J. F. Fennell (1998), AMPTE/CCE-SCATHA simultaneous observations of substorm-associated magnetic fluctuations, *J. Geophys. Res.*, *103*, 4671–4682.

Ohtani, S. I., M. A. Shay, and T. Mukai (2004), Temporal structure of the fast convective flow in the plasma sheet: Comparison between observations and two-fluid simulations, *J. Geophys. Res.*, *109*, A03210, doi:10.1029/2003JA010002.

Panov, E. V., et al. (2010), Multiple overshoot and rebound of a bursty bulk flow, *Geophys. Res. Lett.*, *37*, L08103, doi:10.1029/2009GL041971.

Pritchett, P. L. (2010), Onset of magnetic reconnection in the presence of a normal magnetic field: Realistic ion to electron mass ratio, *J. Geophys. Res.*, *115*, A10208, doi:10.1029/2010JA015371.

Pritchett, P. L., and F. V. Coroniti (2010), A kinetic ballooning/interchange instability in the magnetotail, *J. Geophys. Res.*, *115*, A06301, doi:10.1029/2009JA014752.

Runov, A., V. Angelopoulos, M. I. Sitnov, V. A. Sergeev, J. Bonnell, J. P. McFadden, D. Larson, K.-H. Glassmeier, and U. Auster (2009), THEMIS observations of an earthward-propagating dipolarization front, *Geophys. Res. Lett.*, *36*, L14106, doi:10.1029/2009GL038980.

Runov, A., et al. (2011), Dipolarization fronts in the magnetotail plasma sheet, *Planet. Space Sci.*, *59*, 517–525.

Russell, C. T., and R. L. McPherron (1973), The magnetotail and substorms, *Space Sci. Rev.*, *15*, 205–266.

Schödel, R., W. Baumjohann, R. Nakamura, V. A. Sergeev, and T. Mukai (2001), Rapid flux transport in the central plasma sheet, *J. Geophys. Res.*, *106*, 301–313.

Semenov, V. S., T. Penz, V. V. Ivanova, V. A. Sergeev, H. K. Biernat, R. Nakamura, M. F. Heyn, I. V. Kubyshkin, and I. B. Ivanov (2005), Reconstruction of the reconnection rate from Cluster measurements: First results, *J. Geophys. Res.*, *110*, A11217, doi:10.1029/2005JA011181.

Sergeev, V., R. C. Elphic, F. S. Mozer, A. Saint-Marc, and J.-A. Sauvaud (1992), A two-satellite study of nightside flux transfer events in the plasma sheet, *Planet. Space Sci.*, *40*, 1551–1572.

Sergeev, V. A., V. Angelopulous, J. T. Gosling, C. A. Cattell, and C. T. Russell (1996), Detection of localized, plasma-depleted flux tubes or bubbles in the midtail plasma sheet, *J. Geophys. Res.*, *101*, 10,817–10,826.

Sergeev, V., V. Angelopoulos, S. Apatenkov, J. Bonnell, R. Ergun, J. McFadden, D. Larson, R. Nakamura, and A. Runov (2009), Structure of injection front in the flow braking region, *Geophys. Res. Lett.*, *36*, L21105, doi:10.1029/2009GL040658.

Sitnov, M. I., M. Swisdak, and A. V. Divin (2009), Dipolarization fronts as a signature of transient reconnection in the magnetotail, *J. Geophys. Res.*, *114*, A04202, doi:10.1029/2008JA013980.

Slavin, J. A., et al. (2003), Geotail observations of magnetic flux ropes in the plasma sheet, *J. Geophys. Res.*, *108*(A1), 1015, doi:10.1029/2002JA009557.

Sonnerup, B. U. Ö., and M. Scheible (1998), Minimum and maximum variance analysis, in *Analysis Methods for Multi-Spacecraft Data*, edited by G. Paschmann and P. Daly, pp. 185–220, Eur. Space Agency, Noordwijk, Netherlands.

Sormakov, D. A., and V. A. Sergeev (2008), Topology of magnetic flux ropes in the magnetospheric plasma sheet as measured by the Geotail spacecraft, *Cosmic Res.*, *46*, 387–391.

Tsyganenko, N. A. (1995), Modeling the Earth's magnetospheric magnetic field confined within a realistic magnetopause, *J. Geophys. Res.*, *100*, 5599–5612.

Wiltberger, M., T. I. Pulkkinen, J. G. Lyon, and C. C. Goodrich (2000), MHD simulation of the magnetotail during the December 10, 1996, substorm, *J. Geophys. Res.*, *105*, 27,649–27,663.

Zhang, X.-J., V. Angelopoulos, A. Runov, X.-Z. Zhou, J. Bonnell, J. P. McFadden, D. Larson, and U. Auster (2011), Current-carriers near dipolarization fronts in the magnetotail: A THEMIS event study, *J. Geophys. Res.*, *116*, A00I20, doi:10.1029/2010JA015885.

Zhou, M., M. Ashour-Abdalla, X. Deng, D. Schriver, M. El-Alaoui, and Y. Pang (2009), THEMIS observation of multiple dipolarization fronts and associated wave characteristics in the near-Earth magnetotail, *Geophys. Res. Lett.*, *136*, L20107, doi:10.1029/2009GL040663.

Zhou, X.-Z., V. Angelopoulos, V. A. Sergeev, and A. Runov (2010), Accelerated ions ahead of earthward-propagating dipolarization fronts, *J. Geophys. Res.*, *115*, A00I03, doi:10.1029/2010JA015481.

Zhou, X.-Z., V. Angelopoulos, V. A. Sergeev, and A. Runov (2011), On the nature of precursor flows upstream of advancing dipolarization fronts, *J. Geophys. Res.*, *116*, A03222, doi:10.1029/2010JA016165.

Zong, Q.-G., et al. (2004), Cluster observations of earthward flowing plasmoid in the tail, *Geophys. Res. Lett.*, *31*, L18803, doi:10.1029/2004GL020692.

V. Angelopoulos, S. Li, A. Runov, X.-J. Zhang, and X.-Z. Zhou, Institute of Geophysics and Planetary Physics, University of California, 3845 Slichter Hall, Los Angeles, CA 90095, USA. (arunov@igpp.ucla.edu)

J. Bonnell, Space Sciences Laboratory, University of California, Berkeley, CA 94720, USA.

F. Plaschke, Institut für Geophysik und Extraterrestrische Physik, Technische Universität Braunschweig, Braunschweig D-38106, Germany.